Journal of Neutron Research 20 (2018) 11–21
DOI 10.3233/JNR-180057
IOS Press

High pressure cell for Bio-SANS studies under sub-zero temperatures or heat denaturing conditions

S.C.M. Teixeira [a,b,*], J.B. Leão [b], C. Gagnon [b,c] and M.A. McHugh [d]

[a] *Dep. of Chemical and Biomolecular Engineering, University of Delaware, 150 Academy Street, Newark, DE 19716, USA*
[b] *NIST Center for Neutron Research, National Institute of Standards and Technology, 100 Bureau Drive, Gaithersburg, MD 20899, USA*
[c] *Dep. of Materials Science and Engineering, University of Maryland, College Park, MD 20742, USA*
[d] *Dep. of Chemical and Life Science Engineering, Virginia Commonwealth University, 601 West Main Street, Richmond, VA 23284, USA*

Abstract. The 2nd biennial International Society for Sample Environment (ISSE) School included training on high pressure (HP) cells for Soft Matter studies. Neutron research centers are responding to a growing need for HP experimental data, relevant to a broad range of applications in bioscience, biotechnology and others. The importance of disseminating designs and operating protocols, to support concerted efforts towards the advancement of sample environment instrumentation across research centers, was repeatedly acknowledged at the ISSE school. The liquid insertion HP system for SANS, currently used at the NIST Center for Neutron Research for solutions of biological macromolecules, is described here. Emphasis is placed on the context of subzero temperature studies and the design challenges. The current model of the HP system – HP up to 3.5 kbar and $-18°C < T < +80°C$ – uses sample volumes of 2.7 ml to cover an accessible q-range of 0.001–0.6 $Å^{-1}$.

Keywords: High pressure, subzero temperature, Bio-SANS, small angle neutron scattering

1. Introduction

High pressure (HP) can be used to study phase behavior, molecular structure and dynamics under different sample environments [6,12,35,43,50]. Recent developments [33,34] impacted the range of pressures achievable and, consequently, the type of samples of interest. HP instrumentation can now access compressions exceeding the strength of the strongest molecular bond, changing chemical reactivities and enabling the engineering of novel materials with specific functionalities. Advances in HP small angle scattering are due in no small part to efforts carried out by, or in collaboration with academia. Examples include a stroboscopic HP-SANS cell which can apply up to 10 Hz pressure jumps with adjustable amplitude (up to 0.35 kbar) and duration, used for CO_2-emulsions [37], or cells used to study the pore structure of various types of rocks, where small angle scattering techniques have the unique ability to differentiate between open and closed pores [4], among others.

This article concerns static cells designed to work with maximum pressures – typically up to 500 MPa – insufficient to break covalent bonds, which have significantly higher bond dissociation energies. For a review on the effects of HP on molecules at higher pressures see for example [22]. The importance of HP studies on biological macromolecules has long been recognized [25], with early protein folding studies carried out for proteins in the

*Corresponding author. Tel.: (301)975-4404; E-mail: susanat@udel.edu.

1970s [61], and a few complex macromolecular assemblies in the 1990s [52], but protein phase diagrams are still scarce. The barotropic and thermotropic effects on surfactant phases and microemulsions (see for example [23]) also remain largely uncharacterized. Oligomeric assemblies are particularly sensitive to pressure, often dissociating at pressures below 100 MPa. The volume change of protein unfolding can be determined from the derivative of the Gibbs free energy variation with respect to pressure and HP experiments showed that proteins are very poorly compressible.

HP denatures proteins by changing the surrounding solvent, as well as driving changes towards more packing-efficient protein-protein and protein-solvent specific interactions. Pressure ranges below 2 GPa [60] cause changes in secondary to quaternary structural levels that inform assembly pathways and molecular recognition, stir reaction equilibria and probe for the distribution of structural and dynamic states. HP is equally an essential tool in the analyses of structural flexibility versus stability in piezophiles, and how this dichotomy is balanced for survival in extreme environments [24]. In contrast, the barosensitivity of some microorganisms, including the most infectious food-borne pathogens, enables the use of HP processing of food [42,58] and pharmaceuticals [48] (aka Pascalization, particularly useful with temperature-sensitive products) to increase shelf life and in decontamination-processes. Finally it should be noted that developments in molecular biology and industrial techniques [53] have strongly augmented the use of HP in the last decade, both directly, where HP is used in mechanical disruption, and indirectly as a consequence of the techniques deployed [36]. Examples include cell lysis, high-performance liquid chromatography, analytical ultracentrifugation, HP refolding of inclusion bodies [46], HP crystallization [44], incorporation of membrane proteins into nanodiscs [5], and HP crystallography [31]. Increasingly complex samples can now be produced at a range of scales, allowing for sample-consuming techniques to be deployed.

The relatively wide range of cold neutron wavelengths covers sizes from the tens of angstroms to the micrometer range, central to the study of a variety of sample sizes and complexities. Biological macromolecules and their biomimetic counterparts (see for example [2]) often have a hierarchic organization of macroscopic assemblies and aggregates with various levels of order or pattern. Understanding the impact of environmental parameters requires a holistic characterization at various time and space resolutions. Many of the applicable experimental methods are limited by technical difficulties or idiosyncrasies of the probes used (for a discussion see for example [40]) that can alter the sample, incur in molecule size limitations, or impose a high sample cost in terms of amount of material required.

Nowadays, the latter is no longer prohibitive for most neutron techniques [57], yet sample availability remains a major criteria in the applicability of small angle neutron scattering to biological macromolecules (BioSANS): this was one of the reasons to design an improved HP system at the NCNR. In BioSANS the experimental strategy often involves the use of isotope labelling to minimize incoherent scattering background and to highlight certain components of complex samples – contrast variation – which further adds weight to sample volume considerations.

2. High pressure cells for small angle neutron scattering studies

From a thermodynamic point of view, hydrostatic pressure is considered a simple way to perturb a system of interest, requiring relatively little energy to effect changes in biopolymers and being isostatic regardless of the size or shape of the sample. Experimentally, it is a less straightforward perturbation technique, particularly when combined with the need for precise temperature control.

The penetrating power of neutrons affords significant flexibility in terms of the mechanical properties of the materials that can be used. The choice of material for the body of a HP SANS cell is mostly governed by mechanical strength, wear and corrosion resistance, as well as magnetic permeability. All must meet the specifications for a broad range of temperature and pressure of interest. For BioSANS, many HP cells include optically and neutron transparent windows, to monitor sample loading so that the exposed path is uniformly filled with sample. Windows can also be chosen to be compatible with in-situ complementary techniques, such as light scattering [28] or fluorescence, adding critical versatility to the design. Transducers and fiber optics can be positioned inside the pressure cell, but this option is avoided because the harsh environment often compromises probe sensitivity, accuracy and

lifetime (for a discussion see for example [18,39]). Furthermore, the presence of probes inside the cell tends to significantly increase the sample volume requirements.

Unlike SAXS measurements, where the high flux beams allow for relatively small samples and/or lower concentrations, HP-SANS experiments require a larger illuminated volume. For cell designs that include windows, a compromise must be found to maximize the exposed amount of sample, for better signal-to-noise, while minimizing the amount of unsupported window material that will be withstanding a pressure differential. The next section describes how these criteria were weighted to design a HP-BioSANS pressure system.

2.1. The NIST Center for Neutron Research (NCNR) HP Bio-SANS cell

The HP-cell currently being used for BioSANS data collection at the NCNR (see Fig. 1) for liquid samples is made of a high-nickel-content austenitic steel (Nitronic 50®). Albeit at the cost of more difficult machinability, this material possesses high corrosion resistance and does not become magnetic when cooled to sub-zero temperatures. The maximum allowed working pressure can be calculated using the American Society for Mechanical Engineers code formula:

$$P_{\max} = \frac{2UTS \cdot t}{ID \cdot SF}$$

where *UTS* is the ultimate tensile strength for the high-strength Nitronic 50® bar stock used to make the cell (see Table 1), t is the wall thickness (2.66 cm), *ID* is the inner diameter (4.94 cm) and *SF* is the safety factor. This allows for a $P_{\max}$ of 4.4 kbar (0.44 GPa) at 24°C, using a safety factor of 2.5. The cell is fitted with unclamped optical-grade sapphire windows (1.91 cm outer diameter, by 1.91 ± 0.003 cm thickness) [10]. Window sealing is provided by chemically- and temperature-compatible elastomeric O-rings. For each of the sapphire windows, a silicone ring (70 Shore A durometer hardness, Silicone FDA) contacts the sapphire directly. To prevent extrusion failure, a second Buna-N 90 Contoured back-up O-ring is also present (flat side facing the end-cap of the cell: see Fig. 2).

The empty HP-SANS cell transmissions (Table 2) are above 80% for the most common configurations used at the NCNR NGB30 SANS instrument (corresponding to wavelengths of 6 Å and 8.4 Å) [16]. The instrument configurations used cover a q-range of 0.001–0.6 $Å^{-1}$, where the momentum transfer is defined as a function of

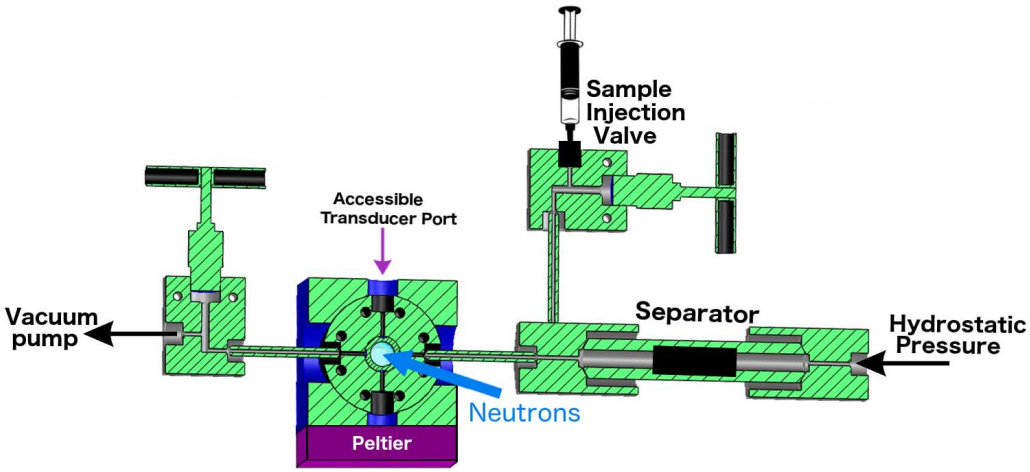

Fig. 1. Schematics of a cut of the LIPSS system (not drawn to scale; the authors are available to provide more information on the real-scale design dimensions as necessary) seen from "the neutron eye". The bottom Peltier label indicates the general position of the group of 4 Peltiers.

Table 1

Typical ultimate tensile strength of high-strength Armco Nitronic 50 bars (from Armco Product Data Bulletin No. S-38, 1986) and calculated maximum allowable working pressures, assuming a safety factor of 2.5. The effects of thermal expansion were not taken into consideration

Temp. (°C)	*UTS* (psi)	P_{max} (kbar)
−73	169,900	5.0
24	150,000	4.4
93	135,000	4.0
204	124,000	3.6
316	117,000	3.4

Table 2

Empty cell transmission measurements and corresponding configurations measured at the NGB30-SANS instrument, at the NCNR, using a 1 mm cell path length. A 0.114 m beam defining aperture was used (positioned just before the cell)

Transmission (%)	Sample-to-Detector Distance (SDD) and configuration
87.6 ± 0.9	SDD 1.33 m, detector offset 0.25 m, λ = 4 Å ($\Delta\lambda/\lambda = 12.5\%$)
80.9 ± 0.3	SDD 1.33 m, detector offset 0.25 m, λ = 6 Å ($\Delta\lambda/\lambda = 12.5\%$)
80.9 ± 0.3	SDD 4 m, no detector offset, λ = 6 Å ($\Delta\lambda/\lambda = 12.5\%$)
80.9 ± 0.3	SDD 13.17 m, no detector offset, λ = 6 Å ($\Delta\lambda/\lambda = 12.5\%$)
74.3 ± 0.7	SDD 13.17 m, no detector offset, λ = 8.4 Å ($\Delta\lambda/\lambda = 12.5\%$).

wavelength (λ) and the scattering angle (2θ):

$$q = \frac{4\pi}{\lambda} \sin\theta$$

Besides relatively transparent to cold neutrons, sapphire is chemically and mechanically resistant. Sapphire offers a very high modulus of rupture: the windows are rated to a rupture modulus strength M of 6.9 kbar (0.69 GPa) [15] and have an unsupported area of 1.27 cm^2. For circular windows, the desired thickness t can be calculated using the equation [19]:

$$t = r \cdot \sqrt{(P \cdot K \cdot SF)/M}$$

where r is the unsupported window radius, P is the pressure differential, K is an empirical constant for circular windows and SF was set to 10 for the sapphire windows. To prevent elastic deformation, the maximum stress applied must be smaller than the rupture modulus by an amount defined by the safety factor so that:

$$S_{max} = M/SF$$

Each window is retained by an end-cap with a 30° included-angle cone that allows a neutron beam to exit the scattering cell at a maximum angle of 15° relative to the window surface, and small angle scattering data to be recorded up to 0.6 $Å^{-1}$, using a neutron wavelength of 4 Å on the NBG30 SANS instrument with a detector offset for the highest angle configuration. The neutron path length across the sample is defined by an edge on an inner sleeve – see Fig. 2 – adjustable to multiples of 1.0 mm for optimal thickness (up to 5.0 mm). The sapphire windows are placed on opposite sides of the sleeve and pushed to the center until they sit on the inner edge (spaced by a distance equal to the thickness of the edge). With the present design, the neutron path length through the cell can increase by several percent for path lengths less than 3.0 mm at 300 MPa internal cell pressure, due to the elastic deformation caused by the windows pushing against the end caps. The window displacement can be easily determined as a function of pressure and temperature [13] using a high-resolution indicator gauge (Starrett Co.,

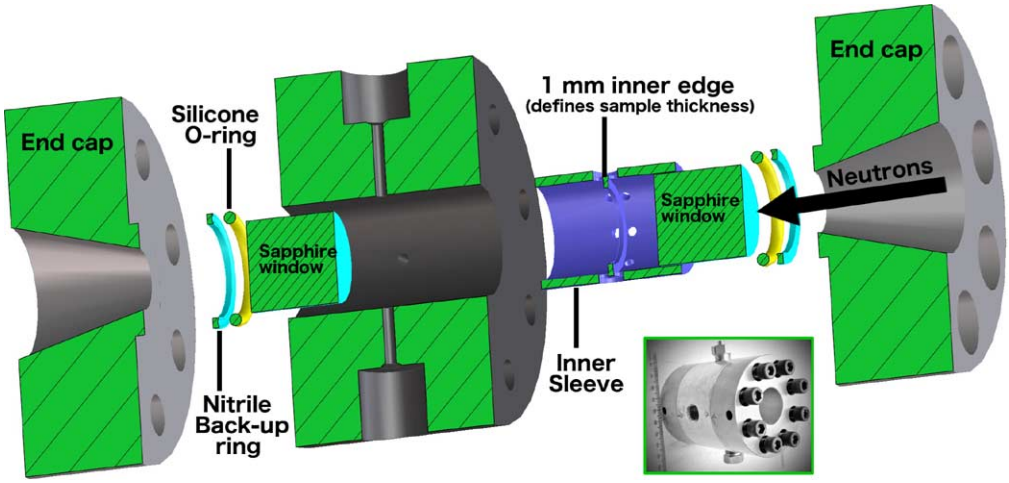

Fig. 2. "Exploded" schematics of the core body of the pressure cell. The small inset shows a photograph of the core body of the cell once assembled, before it is put in position inside the temperature jacket and connected to the LIPSS system. The drawing is scaled for clarity, the authors are available to provide the real-scale dimensions as necessary.

model 25-881). Alternatively, the amount of elastic deformation can be significantly reduced if the end caps are machined from a metal that is harder than Nitronic 50®, such as a grade of Inconel® (austenitic nickel-chromium-based superalloys).

2.2. *Heat vs sub-zero temperature environments*

Heat denaturation (often referred to as thermal denaturation) of a protein typically causes partial or complete unfolding of the secondary and tertiary structures. The temperature increase may or may not lead to complete loss of function. A well-known example is the effect of boiling on eggs, which can also be used to denature epitopes that trigger allergenic responses [49]. Unfolding through heat denaturation is mostly entropy-driven and often causes the irreversible onset of aggregation, due to hydrophobic interactions between denatured proteins. The presence of intermolecular interactions significantly complicates the phase diagram of proteins and most biomolecules (for a review see [54]): for a clearer picture of protein stability, both heat and cold denaturation must be investigated, as clearly shown by studies on the fortuitous cases where cold denaturation occurs at temperatures above freezing [45].

The mid-point of cold denaturation of a native protein at sub-zero temperatures poses experimental challenges and adds effects from the formation and presence of ice. This can be, in part, circumvented through the use of anti-freezing agents, or through destabilizing agents (pH, alcohols, etc) that cause a shift of the cold denaturation to temperatures above freezing. Such strategies however introduce external factors that can induce non-native interactions. The combined use of HP and subzero temperatures offers an alternative, applicable to techniques that would otherwise be hampered by the presence of crystalline ice in the samples under study. This is a particularly important capability for modern biophysics and nanotechnology, where hot- and cold-denaturation studies can be contrasted to probe the energy landscape of biological macromolecules [20,30], and to assist in the design of synthetic routes and studies of new nanomaterials [26,50].

At the NCNR, a thermoelectric-based system [41] has been developed to drive the temperature of the HP-SANS cell in the range 255 K $\leqslant T \leqslant$ 353 K. A combination of four commercially available thermoelectric devices (Peltiers) – capable of expelling the equivalent of 750 Watts of heat from the hot side while removing upwards of 450 Watts from the cold side – is used to set the temperature on the HP-SANS cell. The Peltiers are individually controlled for maximum efficiency. The expelled excess heat is removed via a heat exchanger connected to a silicon oil recirculating bath. 100 Ohms platinum resistance temperature detectors (Pt-100 RTDs) were placed at the top

port of the cell body (for in-situ measurements, see Fig. S1 and discussion in the Supplementary Information), as well as positions on four corners of the cell, to calibrate the sample temperature in terms of offsets at relevant cell positions and equilibration times. Below 2 kbar, the sample temperature can be lowered from room temperature to a uniform temperature across the cell of 255 K ($\pm$ 0.5 K) in 80 minutes. This was verified using readings directly at the sample position. Cooling is significantly slower for sub-zero temperatures and under pressures above 2 kbar (see Supplementary Information).

2.3. Operating the liquid insertion pressure system for SANS (LIPSS)

As shown in Fig. 1, LIPSS is connected to the body of the HP-SANS cell through two ports. One port is connected to a stainless-steel media separator designed for pressures up to 400 MPa, where a piston isolates the pressurizing medium from the sample. O-rings are set in place to ensure sealing under hydrostatic conditions, while a stainless-steel spring on the sample side ensures the separator is driven to its starting position before sample injection. The medium used up to present is degassed ultrapure water, pressurized using a screw-type positive displacement pressure generator. Water has the advantage of causing almost immediately noticeable effects on the experimental data in case of a separator leak, while mixing with the sample does not typically cause irreparable damage. Other hydrostatic pressure media, such as a 4:1 methanol:ethanol mixture, alkane based fluids, or fluorinated aliphatic compounds should be considered for increased lifetime of the pressurizing system materials (for a discussion on the respective advantages see, for example, [59]).

The pressurizing fluid is fed to the separator through a HP cable connected to the SANS sample chamber. The pressurizing and Peltier systems can both be software controlled, activated through commands directly programmable on the SANS data collection software available at the NCNR. The sample injection port is positioned directly on the separator piece, to minimize sample volume requirements. On the opposite side of the separator and injection ports, the cell body is connected to LIPSS through a second port, for access to a vacuum pump. This feature of the system is paramount to assist with sample loading. Using a connection to a vacuum pump, the system may be flushed with cleaning agents and dried for background measurements prior to SANS data collection. With the system under vacuum (the valve on the pump side is closed before data collection), the injection valve is open and the sample is introduced in LIPSS. This method ensures that the full system – 2.7 ml for non-viscous D_2O solutions – is filled with sample and minimizes the presence of air bubbles. Up to 2 ml of the sample volume is recoverable after data collection. The cell body is demountable from the LIPSS system for extensive cleaning and drying while a second cell body is loaded. The LIPSS system frame is locked in place and ensures that alignment in the neutron beam is retained for the second cell body, to minimize dead-time between samples.

The compactness of LIPSS, with total dimensions near those of a regular SANS sample changer, make it easy to assemble in a standard sample chamber where the entire setup can be placed under vacuum. This eliminates the presence of air in the neutron path and, more importantly, allows for lower temperatures to be accessed without condensation of water or solidification of ice on the system surfaces.

2.4. HP-SANS profiles on a standard sample

The LIPSS system was used on a standard protein to assess the required exposure times and protocols for a representative biological sample: a relatively small macromolecule that has been well characterized in a range of environments. The chosen sample was the NIST monoclonal antibody (NISTmAb) reference material [51], a recombinant humanized immunoglobulin (IgG1κ) expressed in murine suspension culture. After brief centrifugation, the samples were injected and data were collected on 5 mg/ml NISTmAb, dissolved in a ^2H_2O buffer containing 12.5×10^{-3} mol/L of L-histidine and 12.5×10^{-3} mol/L of L-histidine HCl, at pD 6.0. Figure 3 shows scattering profiles for the NISTmAb data at atmospheric pressure and at 150 MPa (1500 bar), illustrating the data quality achievable. Given its direct relevance for the biopharmaceutical industry, an extensive report on the HP and temperature effects on the NISTmAb will be reported elsewhere.

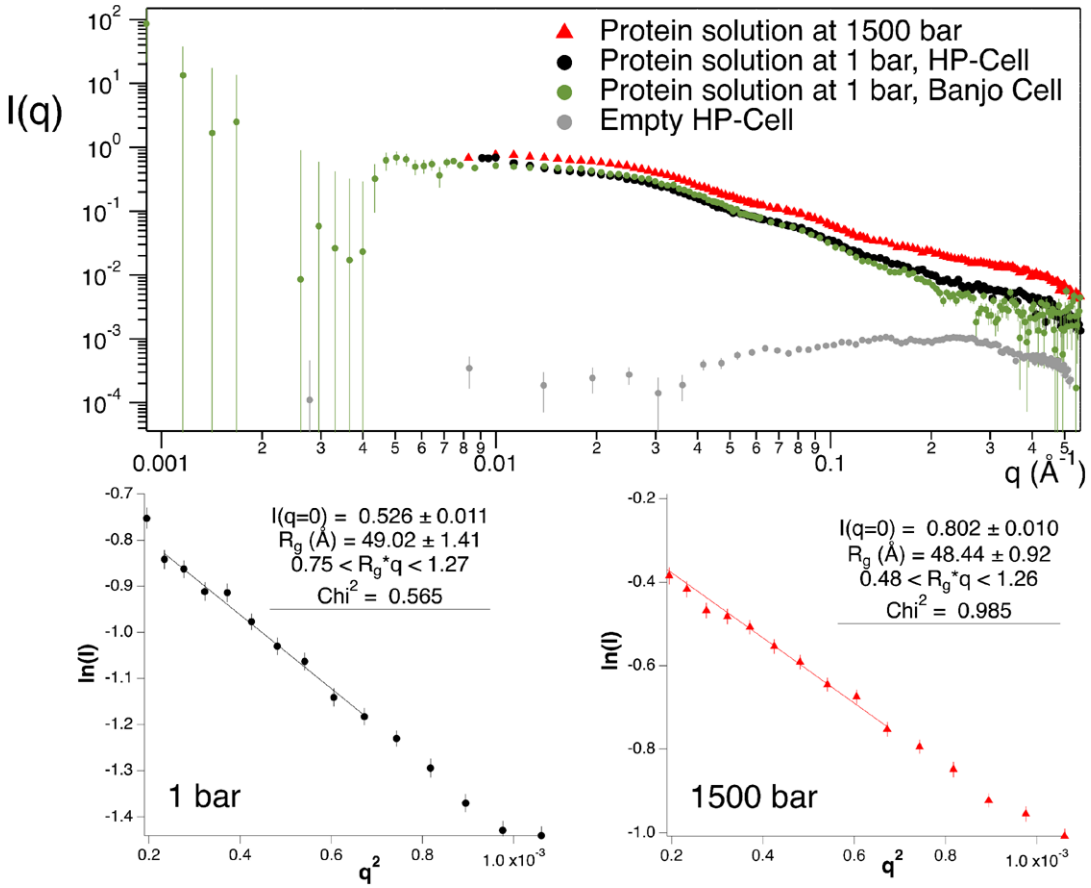

Fig. 3. Example of HP-SANS scattering profiles measured at 22°C for a solution of 5 mg/ml of NISTmAb protein at two different pressures, measured down to 0.01 Å^{-1} in the HP-SANS cell (see also online color version). A profile measured to lower q, using a standard SANS Banjo cell at ambient conditions, is also shown for comparison. Scattering of the empty cell (subtracted by the open beam scattering and measured using the same exposure times as the sample) is also shown. Guinier fits and the corresponding parameters are shown for the two pressures as labelled. The error bars correspond to one standard deviation of uncertainty.

The HP-SANS data were collected on the NGB30 SANS instrument [16] at the NCNR, using a sample aperture of 9.5 mm and a sample thickness of 1 mm. Scattered neutrons were detected with a 64 cm × 64 cm 2D position-sensitive detector with 128 × 128 pixels. To cover a q-range of 0.01–0.6 Å^{-1}, the following configurations were used: low-q (6 Å neutron wavelength, sample to detector distance SDD 13 m), medium-q (6 Å, SDD 4 m) and high-q (4 Å, SDD 1 m and a detector offset of 25 cm). For reference, data were collected for the NISTmAb sample in the pressure cell at atmospheric pressure and temperature conditions (see Fig. 3). The pressure was then increased in steps of 50 MPa, with 5 minutes of equilibration per step. An equilibration time of 30 minutes was used for the final pressure (150 MPa, i.e. 1500 bar) and temperature condition. Neutron exposures of 20 minutes, 15 minutes and 10 minutes were used for the low-, medium- and high-q configurations, respectively. Data were reduced, subtracted, merged and fitted using Igor Pro 7 (WaveMetrics, Lake Oswego, OR) and the NCNR Igor Macros [27]. Data were corrected for scattering from the empty HP cell, stray neutrons and non-uniform detector response. Scattering was normalized to the incident beam flux and radially averaged to obtain the scattering intensity, $I(q)$ versus q. The scattering intensity was further corrected for background scattering from the buffer, to obtain the final scattering intensity for the NISTmAb in solution. The data quality is reflected in the quality of the Guinier fits for the NISTmAb radius of gyration (R_g), which describes the mass distribution of the macromolecule around its

center of gravity: $R_g = 49.02 \pm 1.41$ Å at atmospheric pressure, and $R_g = 48.44 \pm 0.92$ Å at 150 MPa, consistent with values reported in the literature [11,29]. The Guinier analyses [17] were carried out by fitting the data in the low q range limited by $(q \times R_g) < 1.3$, where

$$\ln I(q) = \ln I(0) - \frac{R_g^2}{3} \cdot q^2$$

Data obtained using more standard SANS cells is comparable to that available in the literature [9]. Data collected using 1 mm Banjo cells, as shown for comparison on Fig. 3 (for more details on the data collection for the standard cells at ambient conditions see also the Supplementary Information), is also of similar quality, albeit covering a slightly broader q-range.

3. Discussion

This article places an emphasis on the context of environmental effects on proteins, as representative ubiquitous biological macromolecules. It should be emphasized that the combined use of HP and temperature scans is also relevant to other applications, such as the studies of lipid thermophysical properties and crystallization kinetics [62]. HP-SANS cells with a broad range of pressure and temperature capabilities find applications in the studies of biomembranes, critical to many cellular processes (for a review on HP instrumentation in this context see [7]). Other examples of applications include studies on the self-assembly of the so-called patchy colloidal particles [14,47], or studies of polymer-supercritical fluids [13].

These are exciting times for HP neutron research. Currently available systems for HP-SANS have different characteristics in terms of sample volume, pressure and temperature limits, scattering resolution, etc, collectively providing an expanded range of options that foster studies of novel materials and a deeper understanding of their properties. HP-cell developments for complementary techniques should also be highlighted, such as those available for X-ray scattering [3], fluorescence [32], light scattering [56] or NMR [38], which support and extend the experimental information accessible to SANS. At the NCNR, the LIPSS system offers the unique capability of a broad range of subzero to relatively temperatures: to our knowledge, no other HP-SANS cell offers the combined capability to simultaneously cover the same range of pressure and low temperatures. The Institut Laue Langevin, France, provides HP-SANS cells for up to 500 MPa environments, designed for temperatures above freezing [1,55]. The High Flux Isotope Reactor facilities (Oak Ridge, USA) also offers the possibility of HP environments up to 100 MPa for temperatures above freezing, coupled with the advantage of an HP cell changer that allows for a series of measurements to be pre-programmed on the Bio-SANS instrument [21]. The non-destructive nature of SANS, coupled with its sensitivity to structural changes and ability to highlight components of multimeric assembly of any size, are particularly important for hysteresis studies, as well as in the context of probing slow HP-effects (minutes to hours are often reported, see for example [8]). The availability of more robust cell materials affords a variety of potential improvements that should be taken into consideration for new designs: smaller cells will for example allow for faster temperature equilibration and reduced sample volumes. The technology to synthetically grow single crystal diamonds via chemical vapor deposition is also maturing: larger high-quality diamonds are now possible to grow. This brings the possibility of diamond anvil windows for HP-SANS cells, which withstand larger pressures than sapphire and would allow for larger exit angles, i.e. a broader q-range of SANS to be recorded. Similarly to sapphire, diamond anvil windows further offer the possibility of *in situ* light scattering measurements, a desired addition to a future HP-SANS cell.

Disclaimer

Certain commercial equipment, instruments, suppliers and software are identified in this paper to foster understanding. Such identification does not imply recommendation or endorsement by the National Institute of Standards

and Technology, nor does it imply that the materials or equipment identified are necessarily the best available for the purpose.

Supplementary data

Supplementary Information is available at: http://dx.doi.org/10.3233/JNR-180057.

Acknowledgements

The authors acknowledge John Schiel (NIST, IBBR) for making the protein reference material 8670 available for this study. Access to NGB30 SANS was provided by the Center for High Resolution Neutron Scattering, a partnership between the National Institute of Standards and Technology (NIST) and the National Science Foundation under agreement No. DMR-1508249. We are very grateful to the organizers of the ISSE school, as well as J. Gonthier and E. Lelièvre-Berna (Institut Laue Langevin, France) for their contributions towards the HP-SANS tutorials. We thank the staff at the NIST Center for Neutron Research (NCNR) for advice and useful discussions, in particular to N. Butch, S. Kline, B. Hammouda, Y. Liu and P. Butler. We are very grateful to C. Roberts and D. Gomes (Department of Chemical and Biomolecular Engineering, U. Delaware) for their patience and feedback during the development of the LIPSS system.

References

[1] A new pressure cell for SANS experiments up to 500 MPa, 02/12/2016 [cited 2017]; available from: http://neutronsources.org/news/scientific-highlights/a-new-pressure-cell-for-sans-experiments-up-to-500mpa.html.
[2] A. Aliprandi, M. Mauro and L. De Cola, Controlling and imaging biomimetic self-assembly, *Nature Chemistry* **8** (2016), 10–15. doi:10.1038/nchem.2383.
[3] N. Ando, P. Chenevier, M. Novak, M. Tate and S. Gruner, High hydrostatic pressure small-angle X-ray scattering cell for protein solution studies featuring diamond windows and disposable sample cells, *J. Appl. Cryst.* **41** (2008), 167–175. doi:10.1107/S0021889807056944.
[4] J. Bahadur, C. Medina, L. He, Y. Melnichenko, J. Rupp, T. Blach and D. Mildner, Determination of closed porosity in rocks by small-angle neutron scattering, *Journal of Applied Crystallography* **49**(6) (2016), 2021–2030. doi:10.1107/S1600576716014904.
[5] P. Bhattacharya, S. Grimme, B. Ganesh, A. Gopisetty, J. Sheng, O. Martinez, S. Jayarama, M. Artinger, M. Meriggioli and B. Prabhakar, Nanodisc-incorporated hemagglutinin provides protective immunity against influenza virus infection, *Journal of Virology* **84**(1) (2010), 361–371. doi:10.1128/JVI.01355-09.
[6] P.W. Bridgman, The coagulation of albumen by pressure, *Journal of Biological Chemistry* **19**(4) (1914), 511–512.
[7] N. Brooks, Pressure effects on lipids and bio-membrane assemblies, *IUCrJ* **1**(6) (2014), 470–477. doi:10.1107/S2052252514019551.
[8] R. Buckow, J. Wendorff and Y. Hemar, Conjugation of bovine serum albumin and glucose under combined high pressure and heat, *J. Agric. Food Chem.* **59** (2011), 3915–3923. doi:10.1021/jf104336w.
[9] M. Castellanos, S. Howell, D. Gallagher and J. Curtis, Characterization of the NISTmAb reference material using small-angle scattering and molecular simulation, *Anal. Bioanal. Chrm.* **410** (2018), 2141–2159. doi:10.1007/s00216-018-0868-2.
[10] J. Chervin, G. Syfosse and J. Besson, Mechanical strength of sapphire windows under pressure, *Review of Scientific Instruments* **65** (1994), 2719–2725. doi:10.1063/1.1145206.
[11] N. Clark, H. Zhang, S. Krueger, H. Lee, R. Ketchem, B. Kerwin, S. Kanapuram, M. Treuheit, A. McAuley and J. Curtis, Small-angle neutron scattering study of a monoclonal antibody using free-energy constraints, *J. Phys. Chem. B* **117**(45) (2013), 14029–14038. doi:10.1021/jp408710r.
[12] W. David and R. Ibberson, High-pressure, low-temperature structural studies of orientationally ordered C60, *J. Phys. Condens. Matter* **5** (1993), 7223–7228.
[13] T.P. Dinoia, C. Kirby, J.H. van Zanten and M.A. McHugh, SANS study of polymer-supercritical fluid solutions: Transitions from liquid to supercritical fluid solvent quality, *Macromolecules* **33** (2000), 6321–6329. doi:10.1021/ma000240z.
[14] G. Doppelbauer, E. Bianchi and G. Kahl, Self-assembly scenarios of patchy colloidal particles in two dimensions, *Journal of Physics: Condensed Matter* **22** (2010), 12.
[15] Esco Optics Catalog if Standard and custom optical components [cited 2017]; available from: https://escooptics.com/pages/catalog.

[16] C.J. Glinka, J. Barker, B. Hammouda, S. Krueger, J.J. Moyer and W.J. Orts, The 30 m small-angle neutron scattering instruments at the National Institute of Standards and Technology, *J. Appl. Cryst.* **31** (1998), 430–435. doi:10.1107/S0021889897017020.
[17] A. Guinier and G. Fournet, *Small-Angle Scattering of X-Rays*, G. Fournet, ed., Structure of Matter, Wiley, University of Michigan, 1955.
[18] Z. Guo, C. Lu, Y. Wang, D. Liu, M. Huang and X. Li, Design and experimental research of a temperature compensation system for silicon-on-sapphire pressure sensors, *IEEE Sensors Journal* **17**(3) (2017), 709–715. doi:10.1109/JSEN.2016.2633324.
[19] D.C. Harris, *Materials for Infrared Windows and Domes, Properties and Performance*, SPIE Optical Engineering Press, Bellingham, Washington, USA, 1999.
[20] A. Hédoux, Y. Guinet and L. Paccou, Analysis of the mechanism of lysozyme pressure denaturation from Raman spectroscopy investigations, and comparison with thermal denaturation, *J. Phys. Chem. B* **115** (2011), 6740–6748. doi:10.1021/jp2014836.
[21] W. Heller, G. Lynn, V. Urban, K. Weiss and D. Miles, The Bio-SANS small-angle neutron scattering instrument at Oak Ridge National Laboratory, *Neutron News* **19**(2) (2008), 22–23. doi:10.1080/10448630801975692.
[22] R.J. Hemley, Effects of high pressure on molecules, *Annu Rev Phys Chem* **51** (2000), 763–800. doi:10.1146/annurev.physchem.51.1.763.
[23] *High Pressure Bioscience and Biotechnology: Proceedings of the 2nd International Conference on High Pressure Bioscience and Biotechnology*, Springer-Verlag, Dortmund, Berlin, Heidleberg 2002.
[24] Q. Huang, J. Rodgers, R. Hemley and T. Ichiye, Extreme biophysics: Enzymes under pressure, *Journal of Computational Chemistry* **38** (2017), 1174–1182. doi:10.1002/jcc.24737.
[25] W. Kauzmann, Thermodynamics of unfolding, *Nature* **325** (1987), 763–764. doi:10.1038/325763a0.
[26] T. Kimura, Y. Nibe, S. Funamoto, M. Okada, T. Furuzono, T. Ono, H. Yoshizawa, T. Fujisato, K. Nam and A. Kishida, Preparation of a nanoscaled poly(vinyl alcohol)/hydroxyapatite/DNA complex using high hydrostatic pressure technology for in vitro and in vivo gene delivery, *Journal of Drug Delivery* **2011** (2011), 8.
[27] S.R. Kline, Reduction and analysis of SANS and USANS data using Igor Pro, *J. Appl. Crystallography* **39**(6) (2006), 895–900. doi:10.1107/S0021889806035059.
[28] J. Kohlbrecher, A. Bollhalder, R. Vavrin and G. Meier, A high pressure cell for small angle neutron scattering up to 500 MPa in combination with light scattering to investigate liquid samples, *Review of Scientific Instruments* **78**(125101) (2007), 1–6.
[29] N. König, M. Paulus, K. Julius, J. Schulze, M. Voetz and M. Tolan, Antibodies under pressure: A small-angle X-ray scattering study of immunoglobulin G under high hydrostatic pressure, *Biophysical Chemistry* **231** (2017), 45–49. doi:10.1016/j.bpc.2017.05.016.
[30] S. Kunugi and N. Tanaka, Cold denaturation of proteins under high pressure, *Biochimica et Biophysica Acta* **1595** (2002), 329–344. doi:10.1016/S0167-4838(01)00354-5.
[31] K. Kurpiewska, K. Dziubek, A. Katrusiak, J. Font, M. Ribò, M. Vilanova and K. Lewiński, Structural investigation of ribonuclease A conformational preferences using high pressure protein crystallography, *Chemical Physics* **468** (2016), 53–62. doi:10.1016/j.chemphys.2016.01.010.
[32] A. Maeno and K. Alasaka, High-pressure fluorescence spectroscopy, in: *High Pressure Bioscience*, H.M.K. Akasaka, ed., Subcellular Biochemistry, Springer, Dordrecht, 2015, pp. 687–705.
[33] H.-K. Mao, X.-J. Cehn, Y. Ding, B. Li and L. Wang, Solids, liquids, and gases under high pressure, *Reviews of Modern Physics* (2017).
[34] H.-K. Mao, B. Chen, J. Chen, K. Li, J.-F. Lin, W. Yang and H. Zheng, Recent advances in high-pressure science and technology, *Matter and Radiation at Extremes* **1** (2016), 59–75. doi:10.1016/j.mre.2016.01.005.
[35] R.E. Marquis, High-pressure microbial physiology, *Adv Microb Physiol* **14**(11) (1976), 159–241. doi:10.1016/S0065-2911(08)60228-3.
[36] F. Meersman and P. McMillan, High hydrostatic pressure: A probing tool and a necessary parameter in biophysical chemistry, *Chem. Commun.* **50** (2014), 766–775. doi:10.1039/C3CC45844J.
[37] A. Müller, Y. Pütz, R. Oberhoffer, N. Becker, R. Strey, A. Wiedenmann and T. Sottmann, Kinetics of pressure induced structural changes in super- or near-critical CO_2-emulsions, *Phys. Chem. Chem. Phys.* **16** (2014), 18092–18097. doi:10.1039/C3CP53790K.
[38] L.M. Nguyen and L. Roche, High-pressure NMR techniques for the study of protein dynamics, folding and aggregation, *J. Magnetic Resonance* **277** (2017), 179–185. doi:10.1016/j.jmr.2017.01.009.
[39] Z. Niu, Y. Zhao and B. Tian, Design optimization of high pressure and high temperature piezoresistive pressure sensor for high sensitivity, *Review of Scientific Instruments* **85**(015001) (2014), 1–8.
[40] E. Nogales, The development of cryo-EM into a mainstream structural biology technique, *Nat. Methods* **13**(1) (2016), 24–27. doi:10.1038/nmeth.3694.
[41] G.S. Nolas, J. Sharp and J. Goldsmid, *Thermoelectrics – Basic Principles and New Materials Developments*, 1st edn, Springer Series in Materials Science, Vol. 45, Springer-Verlag, Berlin, Heidelberg, 2001.
[42] F.A. Oliveira, O.C. Neto, L.M.R. dos Santos, E.H.R. Ferreira and A. Rosenthal, Effect of high pressure on fish meat quality – a review, *Trends in Food Science and Technology* **66** (2017), 1–19. doi:10.1016/j.tifs.2017.04.014.
[43] K. Ostrowska, M. Kropidlowska and A. Katrusiak, High-pressure crystallization and structural transformations in compressed R, S-ibuprofen, *Crystal Growth & Design* **15**(3) (2015), 1512–1517. doi:10.1021/cg5018888.
[44] K. Ostrowska, M. Kropidlowska and A. Katrusiak, High-pressure crystallization and structural transformations in compressed R, S-ibuprofen, *Crystal Growth & Design* **15** (2015), 1512–1517. doi:10.1021/cg5018888.
[45] A. Pastore, S. Martin, A. Politou, K. Kondapalli, T. Stemmler and P. Temussi, Unbiased cold denaturation: Low- and high-temperature unfolding of yeast frataxin under physiological conditions, *J. Am. Chem. Society* **129**(17) (2007), 5374–5375. doi:10.1021/ja0714538.

[46] S. Peternel and R. Komel, Isolation of biologically active nanomaterial (inclusion bodies) from bacterial cells, *Microb Cell Fact* **9** (2010), 66. doi:10.1186/1475-2859-9-66.
[47] Z. Preisler, T. Vissers, F. Smallenburg, G. Munaò and F. Sciortino, Phase diagram of one-patch colloids forming tubes and lamellae, *J. Physical Chemistry B* **117** (2013), 9540–9547. doi:10.1021/jp404053t.
[48] Y. Rigaldie, A. Largeteau, G. Lemagnen, F. Ibalot, P. Pardon, G. Demazeau and L. Grislain, Effects of high hydrostatic pressure on several sensitive therapeutic molecules and a soft nanodispersed drug delivery system, *Pharmaceutical Research* **20**(12) (2003), 2036–2040. doi:10.1023/B:PHAM.0000008054.80136.5a.
[49] P. Rupa, L. Schnarr and Y. Mine, Effect of heat denaturation of egg white proteins ovalbumin and ovomucoid on CD4+ T cell cytokine production and human mast cell histamine production, *J. Functional Foods* **18**(A) (2015), 28–34. doi:10.1016/j.jff.2015.06.030.
[50] A. San-Miguel, Nanomaterials under high-pressure, *Chem Soc Rev* **35**(10) (2006), 876–889. doi:10.1039/b517779k.
[51] *State-of-the-Art and Emerging Technologies for Therapeutic Monoclonal Antobody Characterization – Biopharmaceutical Characterization: The NISTmAb Case Study*, D.L.D.J.E. Schiel and O.V. Borisov, eds, ACS Symposium Series, 2015.
[52] J.L. Silva, D. Foguel, A. Dapoian and P. Prevelige, The use of hydrostatic pressure as a tool to study viruses and other macromolecular assemblages, *Current Opinion in Structural Biology* **6**(2) (1996), 166–175. doi:10.1016/S0959-440X(96)80071-6.
[53] H. Simonin, F. Duranton and M. de Lamballerie, New insights into the high-pressure processing of meat and meat products, *Comprehensive Reviews in Food Science and Food Safety* **11** (2012), 285–306. doi:10.1111/j.1541-4337.2012.00184.x.
[54] L. Smeller, Pressure-temperature phase diagrams of biomolecules, *Biochimica et Biophysica Acta* **1595** (2002), 11–29. doi:10.1016/S0167-4838(01)00332-6.
[55] A. Steinschulte, A. Scotti, K. Rahimi, O. Nevskyi, A. Oppermann, S. Scheneider, S. Bochenek, M. Schulte, K. Geisel, F. Jansen, A. Jung, S. Mallmann, R. Winter, W. Richtering, D. Wöll, R. Schweins and N. Warren, Stimulated transitions of directed nonequilibrium self-assemblies, *Advanced Materials* **29**(43) (2017). doi:10.1002/adma.201703495.
[56] H. Takeno, M. Nagao, Y. Nakayama, H. Hasegawa, T. Hashimoto, H. Seto and M. Imai, High pressure cell for small-angle neutron and light scattering studies of phase transitions in complex liquids, *Polymer Journal* **29**(11) (1997), 931–939. doi:10.1295/polymj.29.931.
[57] S.C.M. Teixeira, J. Ankner, M.C. Belissent-Funel, R. Bewley et al., New sources and instrumentation for neutrons in biology, *Chem. Phys.* **345** (2008), 133–151. doi:10.1016/j.chemphys.2008.02.030.
[58] A. Trujillo, M. Capellas, J. Saldo, R. Gervilla and B. Gamis, Applications of high-hydrostatic pressure on milk and dairy products: A review, *Innovative Food Science and Emerging Technologies* **3** (2002), 295–307. doi:10.1016/S1466-8564(02)00049-8.
[59] T. Varga and A. Wilkinson, Fluorinert as a pressure-transmitting medium for high-pressure diffraction studies, *Review of Scientific Instruments* **74**(10) (2003). doi:10.1063/1.1611993.
[60] R. Winter, Synchrotron X-ray and neutron small-angle scattering of lyotropic lipid mesophases, model biomembranes and proteins in solution at high pressure, *Biochimica Et Biophysica Acta – Protein Structure and Molecular Enzymology* **1595**(1–2) (2002), 160–184. doi:10.1016/S0167-4838(01)00342-9.
[61] A. Zipp and W. Kauzmann, Pressure denaturation of metmyoglobin, *Biochemistry* **12** (1973), 4217–4228. doi:10.1021/bi00745a028.
[62] M. Zulkurnain, F. Maleki and V.M. Balasubramaniam, High pressure processing effects on lipids thermophysical properties and crystallization kinetics, *Food Engineering Reviews* **8**(4) (2016), 393–413. doi:10.1007/s12393-016-9144-4.